



A Closed-Loop Multiscale Model of the Cardiovascular System: Application to Heart Pacing and Open-Loop Response

Caterina Gallo^(✉), Luca Ridolfi, and Stefania Scarsoglio

Politecnico di Torino, 10129 Torino, Italy
caterina.gallo@polito.it

Abstract. A 1D description of the arterial tree is coupled to a lumped parameter model of the remaining circulatory system, resulting in a closed-loop multiscale model of the cardiovascular apparatus. The regulation of the arterial pressure is also implemented through a short-term baroreceptor model. The proposed framework reproduces well the physiological cardiovascular behaviour of an healthy young man and the modelled baroreflex mechanism is effective in adjusting the hemodynamic responses to both heart pacing and open-loop aortic-carotid sinus control.

Keywords: Computational hemodynamics ·
Closed-loop multiscale cardiovascular model · Heart pacing ·
Open-loop control

1 Introduction

Numerous *in-silico* models of the human circulation have been proposed for a variety of clinical applications, helping to explore the genesis and features of cardiac and vascular pathologies, sustain the design of medical devices, foresee the effects of therapeutic actions, and trainee medicine students [1].

Depending on the study to carry out, cardiovascular models of different dimensions, from 0D to 3D, have been developed. In particular, the multiscale modelling approach (i.e., distinct dimensions are used depending on the circulation district to simulate) has demonstrated its effectiveness to describe the whole circulation [2]. In fact, it offers a suitable level of detail for each cardiovascular region at a reasonable computational cost.

In this work, we present a closed-loop multiscale model of the cardiovascular system, which puts together a 1D representation of the arterial network, a 0D description of the rest of circulation (peripheral arterial vessels, venous, cardiac and pulmonary circulations) and a baroreflex model.

We exploit and combine some modelling solutions introduced by other authors [3–6], obtaining a model which is able to reproduce some complex key characteristics of the cardiovascular system: the propagation and reflection phenomena of pressure and flow waves along the arterial tree, the non-ideal behaviour of cardiac valves, the well-organized structure of micro-circulation groups and venous return, and the short-term regulation mechanism. In addition to the previous models [3–6], we explicitly introduce the contribution of the unstressed volumes of each 0D compartment and adequately scale the time-dependent cardiac parameters with the heartbeat duration (RR). The novelty of

this work consists in the integration and completion of different validated models of the main portions of human circulation, aiming at getting a comprehensive and versatile framework to explore the hemodynamic response in various configurations, from pathological states (such as valvular dysfunctions and cardiac arrhythmias) to different posture and acceleration conditions.

2 Multiscale Mathematical Model

A schematic representation of the 0D–1D multiscale model is provided in Fig. 1. In the following subsections the sub-models are detailed and equations listed.

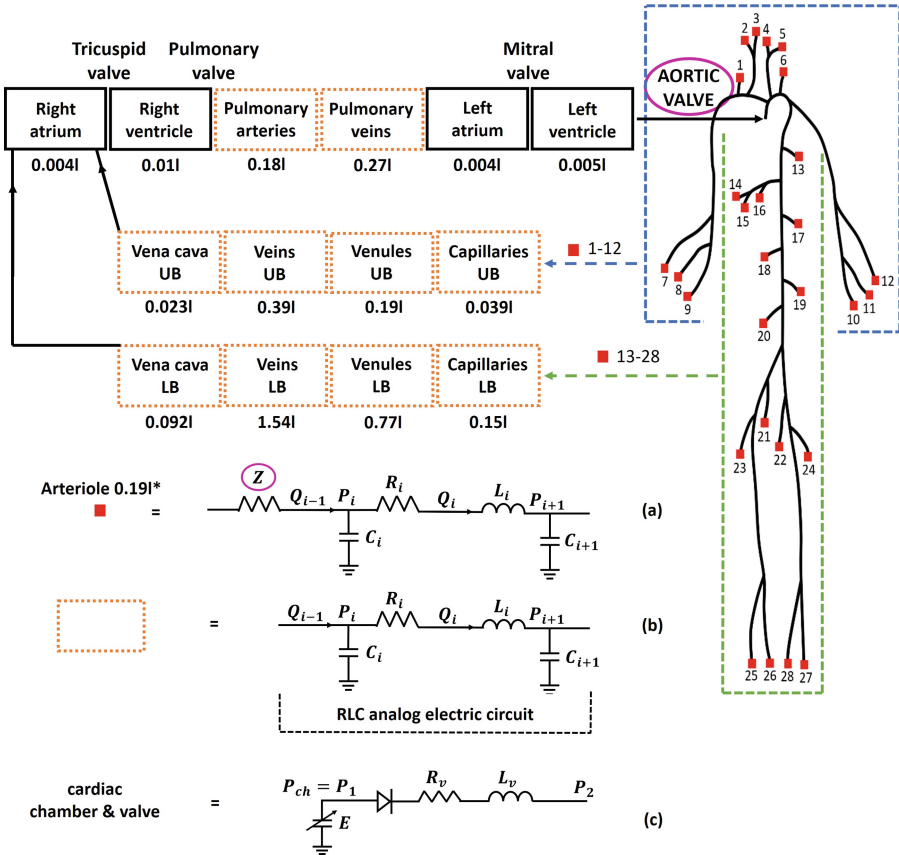


Fig. 1. Schematic representation of the multiscale model, with a sketch of the arterial tree on the right and the structure of all the 0D compartments on the left. The electric circuits corresponding to the lumped elements are given at the bottom (a–c) and the 1D–0D interfaces are highlighted with a purple circle. Values below each 0D compartment are the related unstressed volumes. Regarding the arterioles, the total unstressed volume is indicated (see the asterisk *). This latter is divided among the 28 arteriole groups according to the physiological regional blood volumes [7].

Arterial Tree. Hemodynamics in large-medium arteries is described through the model first proposed by Guala et al. [8], and then used to study the effects of atrial fibrillation on arterial circulation [9]. Mass and momentum balance equations are integrated over the arterial section, leading to the 1D system

$$\begin{cases} \frac{\partial A}{\partial t} + \frac{\partial Q}{\partial x} = 0, \\ \frac{\partial Q}{\partial t} + \frac{\partial}{\partial x} \left(\beta \frac{Q^2}{A} \right) = -\frac{A}{\rho} \frac{\partial P}{\partial x} + N_4, \end{cases} \quad (1)$$

where x and t are the spatial and time coordinates, A is the vascular section, Q is the flow rate, P is the pressure, ρ is the blood density, β is the Coriolis coefficient and N_4 is the viscous term. To close the above system, a constitutive relation for $P = P(A)$, accounting for the anisotropic non-linear viscoelastic behaviour of the arterial walls, is introduced. Details on the parameter settings, which refer to an healthy young man, can be found in [8,9].

Peripheral, Venous and Pulmonary Circulations. Arterioles, capillaries, venous return (venules, veins and venae cavae) and pulmonary circulation (arteries and veins) are simulated adopting different 0D models of similar form (Fig. 1b) [3], provided that arterioles are preceded by the characteristic impedance of the terminating 1D artery (Fig. 1a) [4]. The RLC analog electric circuit of each 0D compartment corresponds to the following system

$$\begin{cases} \frac{dV_i}{dt} = Q_{i-1} - Q_i, \\ \frac{dQ_i}{dt} = \frac{P_i - R_i Q_i - P_{i+1}}{L_i}, \\ P_i = \frac{V_i - V_{i_0}}{C_i}. \end{cases} \quad (2)$$

For the generic i -th compartment, V_i and V_{i_0} are the total and unstressed volumes, Q_{i-1} and Q_i are the flow rates entering and exiting the compartment, while P_i and P_{i+1} are the pressures at the inlet and outlet of the compartment, respectively. R_i (resistance), L_i (inertance), and C_i (compliance) characterize each compartment and are set according to [4] (for arterioles) and [3,6] (for the other lumped elements). V_{i_0} values are reported in Fig. 1 and, together with the overall stressed volume, give a total blood volume equal to 5.5 l.

Heart Chambers. Pressure, P_{ch} , and stressed volume, $(V_{ch} - V_{ch_0})$, of heart chambers are linked through the equation [3,6]

$$P_{ch} = E(V_{ch} - V_{ch_0}) + S\dot{V}_{ch}, \quad (3)$$

where $S = 0.0005P_{ch}$ is the viscoelasticity coefficient of the cardiac wall, \dot{V}_{ch} is the time derivative of V_{ch} , and $E = E_{Ae} + E_B$ is the elastance function. In this

latter expression, E_A and E_B (the amplitude and baseline values of elastance), as well as e (the time-varying elastance function) are chosen as in [3,6]. The time parameters of e are calculated as functions of RR . In particular, durations of contraction and relaxation periods are: $T_{acp} = 0.17RR$ and $T_{arp} = T_{acp}$ [3,4,6] for atria, and $T_{vcp} = 0.3\sqrt{RR}$ [10] and $T_{vrp} = 0.5T_{vcp}$ [10] for ventricles. Contraction and relaxation start at: $t_{ac} = 0.8RR$ and $t_{ar} = t_{ac} + T_{acp}$ for atria, and $t_{vc} = 0RR$ and $t_{vr} = t_{vc} + T_{vcp}$ for ventricles.

Heart Valves. Each cardiac valve is simulated by a pressure-flow model [6,11]. The non-ideal behaviour of the valve is considered and the valve opening angle, θ_v , is calculated based on the rotational inertia (I_{ao}) and forces acting on the valve leaflets - pressure difference across the valve, F_{pr} , dynamic effect of the blood acting on the valve leaflets, F_{bm} , frictional effects of neighbouring tissue resistance, F_{fr} , and vortices downstream of the valve, F_{vo} - namely

$$\begin{cases} L_v \frac{dQ_v}{dt} + R_v Q_v + B_v |Q_v| Q_v = \frac{(1 - \cos(\theta_v))^4}{(1 - \cos(\theta_{max}))^4} (P_1 - P_2), \\ I_{ao} \frac{d^2\theta_v}{dt^2} = F_{pr} + F_{bm} - F_{fr} - F_{vo}. \end{cases} \quad (4)$$

Q_v is the flow rate through the valve, $P_1 - P_2$ is the pressure difference across the valve, and L_v , R_v and B_v stand for the inertance, viscous and turbulent flow separation effects, respectively. All parameters are set as in [6].

Baroreflex Model. We adopt the baroreflex model introduced by Ottesen et al. [12]. Sympathetic, n_s , and parasympathetic activity, n_p , are evaluated as

$$n_s(\bar{p}_{acs}) = \frac{1}{1 + \left(\frac{\bar{p}_{acs}}{\bar{p}_{acs,ref}}\right)^\nu}, \quad n_p(\bar{p}_{acs}) = \frac{1}{1 + \left(\frac{\bar{p}_{acs}}{\bar{p}_{acs,ref}}\right)^{-\nu}}, \quad (5)$$

where ν (here set equal to 7) gives the slope of the n_s and n_p responses, while \bar{p}_{acs} is the aortic-carotid sinus pressure averaged over the cardiac cycle. $\bar{p}_{acs,ref}$ is the baseline value of the average aortic-carotid sinus pressure which, determined at a reference heart rate (HR) of 75 bpm, is equal to 92 mmHg. The efferent responses are described as

$$\frac{dx_j}{dt} = \frac{1}{\tau_j} (-x_j + \alpha_j n_s(\bar{p}_{acs}) - \beta_j n_p(\bar{p}_{acs}) + \gamma_j), \quad (6)$$

where x_j is the generic efferent organ, τ_j is the time delay in the efferent response, α_j and β_j define the weights of n_s and n_p , and γ_j equals x_j when $\bar{p}_{acs} = \bar{p}_{acs,ref}$. Efferent organs are HR, maximum values of right- and left-ventricular elastance ($E_{A_{r,l}}$), arteriole and capillary resistances ($R_{a,c}$), the compliances, and unstressed volumes of venules and veins ($C_{ven,v}$, $V_{0_{ven,v}}$). Baroreflex parameters are indicated in Table 1.

Table 1. Parameters of the baroreflex model for each efferent organ. α , β , γ values and saturation levels (Min. and Max.) of efferent organs are non-dimensional.

Efferent organ	τ [s]	α	β	γ	Min.	Max.
HR	3	0.75	0.75	1	0.25	1.75
$E_{A,rl}$	3	0.40	0	0.80	0.8	1.2
$R_{a,c}$	15	0.80	0	0.60	0.6	1.4
$C_{ven,v}$	30	-0.20	0	1.10	0.9	1.1
$V_{0_{ven,v}}$	30	-0.42	0	1.21	0.79	1.21

Numerical Resolution. The complete model is solved through a Runge-Kutta Discontinuous-Galerkin scheme. Space is discretized according to a Discontinuous-Galerkin approach and dependent variables are advanced in time adopting a two-steps Runge-Kutta explicit scheme. Pressure and flow rate values at the 1D–0D interfaces and at each arterial junction are defined by combining physical and compatibility numerical conditions [8]. Physical conditions are given by: the system (4) at aortic valve, the constitutive equation of the characteristic impedance Z at peripheral arterial vessels, and the conservation of mass and total pressure at arterial bifurcations.

3 Results and Conclusions

Physiological Behaviour. The modelled cardiovascular system well reproduces the physiological hemodynamics of a healthy young man at 75 bpm. Figure 2 shows pressure (a) and flow rate (b) signals at specific arterial sites, evidencing that the propagation phenomena of arterial waves are efficiently reproduced. In fact, moving away from the heart, systolic pressures increase, diastolic pressures decrease, pressure signals delay and steepen, and flow rate signals reduce in amplitude [13]. Figure 2c-d display the pressure and flow rate signals for the lower body venous, V_{LB} , and vena cava, VC_{LB} , compartments. As expected [4, 14], it emerges that pressure is almost constant, while flow rate is still pulsatile along the venous return. Flow rates through cardiac valves (see Fig. 2e) clearly show the typical trasvalvular flow, with the physiological reversal flow as valves close [11].

Baroreflex Efficacy. To demonstrate the reliability of our model, we report two tests about the baroreflex system: (i) the response to heart pacing and (ii) the so-called open-loop case. In heart pacing, a fixed value of HR is externally forced and the response of the remaining effector organs is determined by the baroreflex mechanism [12]. Instead, in the open-loop case, the ratio $\bar{p}_{acs}/\bar{p}_{acs,ref}$ is externally applied. We simulated eight HRs (35, 55, 75, 95, 115, 135, 155 and 175 bpm) in heart pacing and seven ratios $\bar{p}_{acs}/\bar{p}_{acs,ref}$ (from 0.625 to 1.375) in the open-loop analysis.

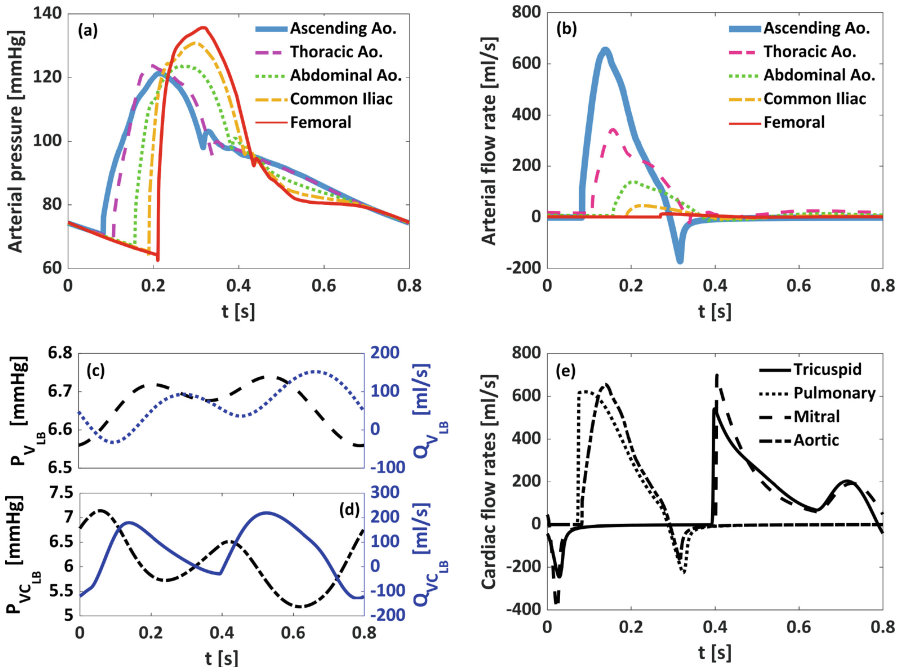


Fig. 2. (a) Arterial pressure and (b) flow rate signals along the aorta. (c)–(d) Pressure (P) and flow rate (Q) signals: (c) lower body venous compartment (V_{LB}), and (d) lower body vena cava compartment (V_{CLB}). (e) Flow rate signals through cardiac valves. All the figures refer to a healthy young man with 75 bpm.

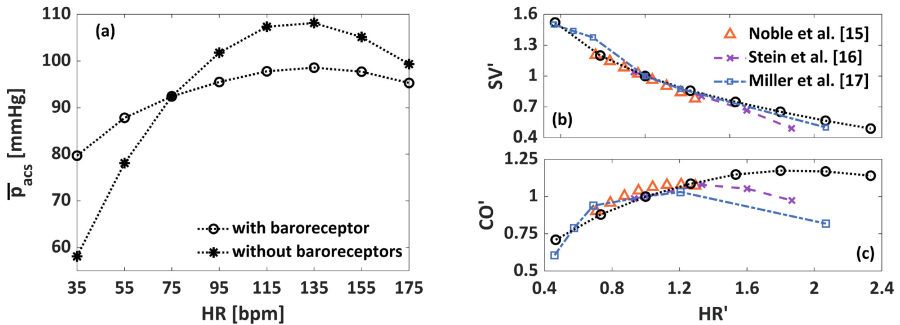


Fig. 3. Heart pacing case. (a) Behaviours of the average aortic-sinus carotid pressure (with and without baroreceptors) with HR. Dependence of the non-dimensional stroke volume (b) and cardiac output (c) on HR. Variables marked with a superscript are non-dimensional. Normalization is referred to the baseline values at 75 bpm for computed results and to the indicated or assumed baseline values for experimental results (provided in dimensional form). Data by Stein et al. [16] refer to human subjects, while data by Noble et al. [15] and Miller et al. [17] are measured on dogs.

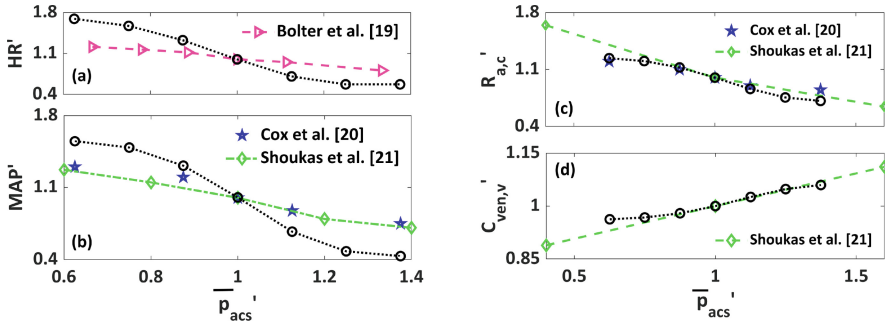


Fig. 4. Open-loop case. Non-dimensional open-loop responses for the (a) heart rate, (b) mean arterial pressure, (c) arterial and capillary resistances, and (d) compliances of venule and venous compartments. Variables marked with a superscript are non-dimensional. Normalization is referred to the baseline values at 75 bpm for computed results and to the indicated or assumed baseline values for experimental results (provided in dimensional form, except in Cox et al. [20]). All experimental data refer to dogs.

Figure 3 shows the results in the case of heart pacing simulation. Panel 3a reports the function $\bar{p}_{acs}(\text{HR})$ with and without baroreceptors, demonstrating that arterial pressure variations are limited by baroreflex as cardiac frequency is altered from the reference value (75 bpm). Figure 3b and c show the behaviours of the stroke volume, SV' , and cardiac output, CO' , as functions of HR' (superscript indicates non-dimensional quantities), together with the experimental data by [15–17]. Results provided by the model are normalized with respect to baseline values at 75 bpm. Instead, dimensional experimental results are normalized with respect to the indicated baseline values (if available) or reasonably assumed baseline values. It is typically reported in literature [18] that SV reduces as HR rises, while CO increases at low HR s, reaches a maximum value for higher HR s (between 90 and 180 bpm) and finally reduces for further HR increments. These trends are reproduced in Fig. 3b and c, where an overall agreement between computed and experimental data is observed. However, the maximum CO predicted by the model (between 135 and 155 bpm) seems to be located at non-dimensional frequencies higher than the ones associated to the experimental measures. This could depend on the way in which HR is modified in the experimental measures (ventricular pacing, atrial pacing, pharmacological agents, exercise, etc.) as well as the experimental conditions (e.g., conscious or anaesthetized subjects) [16]. Moreover, since experimental results are given in dimensional form, there are some difficulties in comparing data from different sources.

Figure 4 refers to the open-loop analysis. The behaviours of HR , mean arterial pressure (MAP), arterial and capillary resistances ($R_{a,c}$), and compliances of venules and veins ($C_{ven,v}$), as functions of \bar{p}_{acs} , are provided in non-dimensional form for computed and experimental results [19–21]. Normalization of both computed and experimental results is done as in the case of heart pacing. One can appreciate a general correspondence between numerical and experimental results,

although some discrepancies emerge. In fact, experimental results are obtained considering only the contribution of carotid sinus pressure in the baroreflex action. By contrast, pressure activating the baroreflex in our model is a combination of both aortic arch and carotid sinus pressures.

Based on the previous results, the proposed model satisfactorily reproduces the most important features of the arterial and venous hemodynamics, cardiac dynamics and short-term regulation mechanisms. Thus, the choice of the sub-models representing each portion of the circulation, their integration into a unique framework, the parameter setting and the numerical resolution of the complete mathematical formulation, lead to an efficient and accurate *in-silico* model of the cardiovascular system.

Next efforts will consist in considering the effects of orthostatic variations, adding the contribution of the gravity, transmural pressures, and venous valves to guarantee unidirectional blood flow from lower to upper body. These additional features will allow one to investigate space-related medical issues, such as the fallouts of long-term microgravity exposure on the human hemodynamics.

Declaration of Interest. The authors declare that they have no conflict of interest.

References

1. Morris, P.D., Narracott, A., von Tengg-Kobligk, H., Silva Soto, D.A., Hsiao, S., Lungu, A., Evans, P., Bressloff, N.W., Lawford, P.V., Hose, D.R., Gunn, J.P.: Computational fluid dynamics modelling in cardiovascular medicine. *Heart* **102**, 18–28 (2016). <https://doi.org/10.1136/heartjnl-2015-308044>
2. Shi, Y., Lawford, P., Hose, R.: Review of zero-D and 1-D models of blood flow in the cardiovascular system. *Biomed. Eng. Online* **10**, 33 (2011). <https://doi.org/10.1186/1475-925X-10-33>
3. Liang, F., Takagi, S., Himeno, R., Liu, H.: Multi-scale modeling of the human cardiovascular system with applications to aortic valvular and arterial stenoses. *Med. Biol. Eng. Comput.* **47**, 743–755 (2009). <https://doi.org/10.1007/s11517-009-0449-9>
4. Liang, F.Y., Takagi, S., Himeno, R., Liu, H.: Biomechanical characterization of ventricular-arterial coupling during aging: a multi-scale model study. *J. Biomech.* **42**, 692–704 (2009). <https://doi.org/10.1016/j.jbiomech.2009.01.010>
5. Blanco, P.J., Trenhago, P.R., Fernandes, L.G., Feijóo, R.A.: On the integration of the baroreflex control mechanism in a heterogeneous model of the cardiovascular system. *Int. J. Numer. Meth. Biomed. Engng.* **28**, 412–433 (2012). <https://doi.org/10.1002/cnm.1474>
6. Blanco, P.J., Feijóo, R.A.: A dimensionally-heterogeneous closed-loop model for the cardiovascular system and its applications. *Med. Eng. Phys.* **35**, 652–667 (2013). <https://doi.org/10.1016/j.medengphy.2012.07.011>
7. Wayson, M.B., Leggett, R.W., Jokisch, D.W., Lee, C., Schwarz, B.C., Godwin, W.J., Bolch, W.E.: Suggested reference values for regional blood volumes in children and adolescents. *Phys. Med. Biol.* **63**, 155022 (2018). <https://doi.org/10.1088/1361-6560/aad313>

8. Guala, A., Camporeale, C., Tosello, F., Canuto, C., Ridolfi, L.: Modelling and subject-specific validation of the heart-arterial tree system. *Ann. Biomed. Eng.* **43**, 222–237 (2015). <https://doi.org/10.1007/s10439-014-1163-9>
9. Scarsoglio, S., Gallo, C., Ridolfi, L.: Effects of atrial fibrillation on the arterial fluid dynamics: a modelling perspective. *Meccanica* **53**, 3251–3267 (2018). <https://doi.org/10.1007/s11012-018-0867-6>
10. Heldt, T., Shim, E.B., Kamm, R.D., Mark, R.G.: Computational modeling of cardiovascular response to orthostatic stress. *J. Appl. Physiol.* **92**, 1239–1254 (2002). <https://doi.org/10.1152/jappphysiol.00241.2001>
11. Korakianitis, T., Shi, Y.: Numerical simulation of cardiovascular dynamics with healthy and diseased heart valves. *J. Biomech.* **39**, 1964–1982 (2006). <https://doi.org/10.1016/j.jbiomech.2005.06.016>
12. Ottesen, J., Olufsen, M., Larsen, J.: *Applied Mathematical Models in Human Physiology*. Society for Industrial and Applied Mathematics, Philadelphia (2004)
13. Caro, C.G., Pedley, T.Y., Schroter, R.C., Seed, W.A.: *The Mechanics of the Circulation*, 2nd edn. Cambridge University Press, New York (2012)
14. Guyton, A., Hall, J.: *Textbook of Medical Physiology*, 11th edn. Elsevier Saunders, Philadelphia (2006)
15. Noble, M.I.M., Trenchard, D., Guz, A.: Effect of changing heart rate on cardiovascular function in the conscious dog. *Circ. Res.* **19**, 206–213 (1966). <https://doi.org/10.1161/01.RES.19.1.206>
16. Stein, E., Damato, A.N.: The relation of heart rate to cardiovascular dynamics. *Circulation* **33**, 925–932 (1966). <https://doi.org/10.1161/01.cir.33.6.925>
17. Miller, D.E., Gleason, W.L., Whalen, R.E., Morris, J.J., McIntosh, H.D.: Effect of ventricular rate on the cardiac output in the dog with chronic heart block. *Circ. Res.* **10**, 658–663 (1962). <https://doi.org/10.1161/01.RES.10.4.658>
18. Berglund, E., Borst, H.G., Duff, F., Schreiner, G.L.: Effect of heart rate on cardiac work, myocardial oxygen consumption and coronary blood flow in the dog. *Acta Physiol.* **42**, 185–198 (1958). <https://doi.org/10.1111/j.1748-1716.1958.tb01551.x>
19. Bolter, C.P., Ledson, J.R.: Effect of cervical sympathetic nerve stimulation on canine carotid sinus reflex. *Am. J. Physiol.* **230**, 1026–1030 (1976). <https://doi.org/10.1152/ajplegacy.1976.230.4.1026>
20. Cox, R.H., Bagshaw, R.J.: Baroreceptor reflex control of arterial hemodynamics in the dog. *Circ. Res.* **37**, 772–786 (1975). <https://doi.org/10.1161/01.RES.37.6.772>
21. Shoukas, A.A., Connolly-Brunner, M.: Epinephrine and the carotid sinus baroreceptor reflex. *Circ. Res.* **47**, 249–257 (1980). <https://doi.org/10.1161/01.RES.47.2.249>